Deep Density-aware Count Regressor

CHEN ZHUOJUN georgechenzi@outlook.com

Confidential submitted paper For presentation by the author CHEN ZHUOJUN only. Do not distribute

Abstract

We seek to improve crowd counting as we perceive the limits of currently prevalent counting by density map estimation approach on both prediction accuracy and time efficiency. We propose a novel deep CNN which focuses on predicting a more accurate global count while optionally producing multi-scale density maps in a much more efficient way. We introduce multilayer gradient fusion for training a density-aware count regressor. More specifically, on training stage, a backbone network receives gradients from multiple branches to learn the density information, whereas those branches are to be detached to accelerate inference. By taking advantages of such method, our model outperforms the state-of-the-art methods with 27.5%, 2.7% and 14.3% lower MAE on UCF-ONRF, Shanghai Tech Part A and Part B datasets respectively. Our code and models will be publicly available at: https://github.com/[anonymised].

1. Introduction

Crowd counting is a task to count people in image. It is mainly used in real-life for automated public monitoring such as surveillance and traffic control. In recent years, crowd counting has drawn more attention from computer vision researchers and has been in significant progress. However, the task is riddled with many challenges due to the presence of various complexities such as non-uniform density, intra- and inter-scene variations in scale and perspective, and cluttering [8, 9]. Figure 1 illustrates some of those challenging scenarios.

Early methods [1,10,12,22,34] attempt to solve crowd counting problem by detecting each individual pedestrian in the crowd. These methods often perform poorly in the face of the above-mentioned conditions. The recent development of crowd counting comes from DNN-based methods which have achieved commendable performance. These methods [4,5,6,7] concentrate on generating the demanding density maps before integrating them to the count. They are therefore categorised into density mapbased methods. However, density maps have yet, in effect, to show too much importance in practice except for



150

151

152

153

154

155

156

157

158

159 160

161

162

163

164

165

166

167

168

169

170

171

172

173

174

175

179

189

Figure 1. Representative images for challenges of non-uniform density, intra- and inter-scene variations in scale and 177 perspective, and cluttering. In the figure, GT. means ground truth 178 and P. means prediction made by out method.

opportunely providing for demonstration, but are expensive 180 to compute, and their quality is difficult to guarantee. 181 Meanwhile, methods that regress the global count directly 182 have remained untouched for a while in research frontiers. 183

There is experiment in [29] suggesting that direct count 184 regression may have comparable performance to density 185 map-based methods. Raising state-of-the-art performances 186 in many works, density maps have shown undeniable 187 contribution to the improvement of count prediction. One 188 advantage of density map-based methods may be that information with respect to location, scale alike is fed to the network through density supervision. Consequently, multiscale or multi-column architectures [4,5,6,11,15] are usually adopted to fuse features from different scales to capture these kinds of information.

Still, there exists two main drawbacks: first, computational cost drastically increases along with the growth of number of columns; second, useful information 196 learned by low-level detectors might be lost through 197 forward propagation. Likewise, supervision information 198 contained in gradients would be attenuated through 199 backward propagation, making low-level detectors difficult to learn.

To address these problems, we propose a novel Gradient Fusion based model called DeepCount for crowd counting (network architecture shown in Figure 2), making efforts to both avert expenditure of multi-column architecture and improve precision. As in Figure 2, our proposed model contains a backbone network with convolution layers deeply regressing a global count. Some auxiliary modules branch out to produce density maps with corresponding spatial dimensions and to feed gradients back to the backbone. There are five branches having different depths and independent parameters so as to learn features in different aspects. For reducing information loss, each branch will directly access different levels of the backbone to inculcate knowledge to it deeply and make it more perceptive on the density distribution of the image, namely to be density-aware.

In inference phase, the backbone network can be used unaccompanied by branches as a regressor to efficiently predict the global count, or, if needed, with an auxiliary branch to also visualise a density map. Expensive computation is taken out, but with functionality promised.

Compared to other multi-column methods, our model fuses gradients other than features and avoids relying on the hard-to-produce density maps to make prediction, but instead to leverage density maps on training and dismiss them in inference. By so doing, our model is able to incorporate advantages of accuracy, flexibility, and efficiency.

Extensive experimental results on four benchmark datasets demonstrate significant improvements of our method against the state-of-the-art methods on Shanghai Tech Part A, Part B and UCF-QNRF datasets and excellent performance on Mall dataset.

The rest of the paper is structured as follow: we review literatures for crowd counting in section 2; section 3 provides the detailed interpretation of our method; section 4 reports experiment results; in section 5, we further discuss our findings and insights; the paper is to be concluded in section 6.

2. Related works

2.1. Detection-based methods

Early crowd counting methods tend to rely on detection by sliding window approach. Low-level hand-crafted features such as Histograms of Oriented Gradients, silhouette-oriented features are exploited for traditional classifiers such as Support Vector Machine and Random Forest [1, 10, 12, 22, 34]. Following are CNN-based methods (e.g. Faster R-CNN [28]) which have shown credible detection precision [23]. Nonetheless, in such times when the subject of crowd counting was more on the stage of pedestrian detection, performances of these

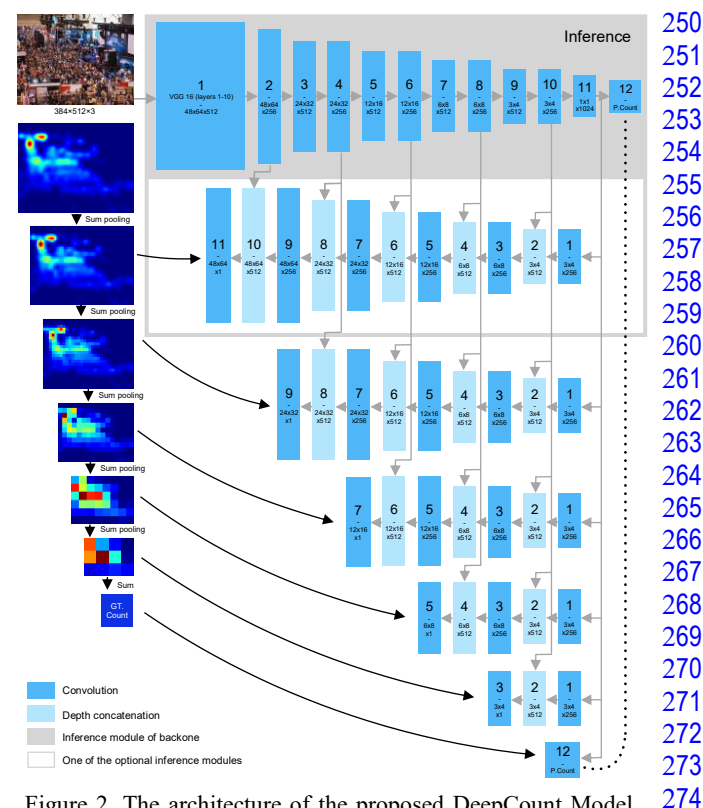


Figure 2. The architecture of the proposed DeepCount Model. Module in the grey box is the backbone regressor, below which are 5 branches predicting density maps. Large-size numbers on the blocks are referred to in detailed configuration in Table 1, while numbers in smaller font indicate the feature map dimensions.

275

276

277

278

279

280

281

282

283

291

294

295

296

297

methods on highly dense crowd scenes were similarly limited.

2.2. Count regression-based methods

Count regression-based methods are proposed to 284 overcome limits encountered by detection-based methods. 285 The idea of these methods is to regress a global count from 286 the input image. There are methods using ridge regression 287 [13, 14], log-linear regression [17] or MLP [20] on low- 288 level hand-crafted features to estimate the count. While 289 these methods work satisfactorily on invariant scenes of sparse density, hand-crafted features can hardly represent enough variance and intricacy in complex counting 292 scenarios. Alternatively, with the development of deep learning, features can be black-boxed and deeply learned to target the goal. Early success of applying deep learning methods on crowd counting would be the end-to-end deep CNN regression model by Wang et al. [18]. Though, deep learning methods quickly narrowed onto density map-based methods which have prevailed over the years since, and it 298 was not until recently in [29] that Idrees et al. report 299 excellent experiment results on global count regression by advanced CNNs: Resnet101 [25] and Densenet201 [26].

Though, their focus is still on density map estimation.

2.3. Density map-based methods

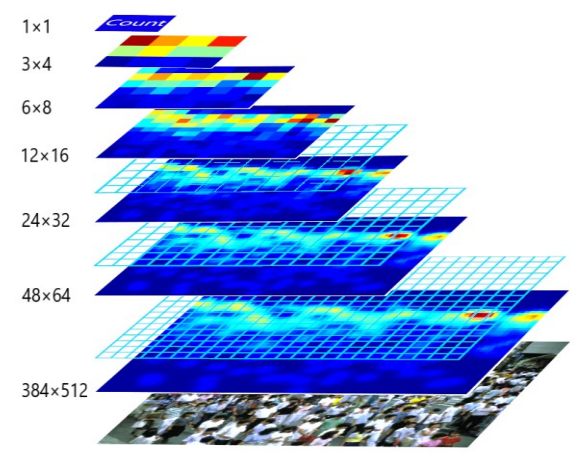
Rodriguez et al. [21] first suggest the use of density map can improve crowd counting results significantly. It is supported by Zhang et al. [7] whose model produces small density map patches as well as the patch count at its last layer. Following this density map approach, Zhang et al. [4] propose a multi-column architecture (MCNN) to also address scale variance of the counting target. Inspired by such, Cao et al. [11] introduce Scale Aggregation Network (SANet) which aggregates multi-scale features and fuses them in every layer. Likewise, Switching-CNN [5] has independent columns of regressors similar to multi-column network with different receptive fields, and ic-CNN [15] aims at predicting high-resolution density maps with two branches. Another set of methods devote themselves to trace context information as well as other abstractions all in a bit to improve the predicted density maps [6, 35, 36, 37]. On the other hand, CSRNet [16] builds dilated convolution layers upon a VGG-16 [19] backbone straightforward without too many manoeuvres, yet it reports excellent results and therefore becomes more practiced at present.

Differently, our method embodies heterogeneity of multi-column methods and straightforwardness of CSRNet, whilst appears as an existence that is both regression-based and density map-based.

3. DeepCount

3.1. Gradient Fusion

We regard our methodology of designing the network as Gradient Fusion. Multi-column methods such as MCNN [4] and CP-CNN [6] are feature fusion methods assembling different columns features from which are fused and gradients to which are separated. Fusing feature maps of multiple columns entails lots of computation overhead since each column cannot be without in order to make prediction. In contrast, the method of gradient fusion fuses only gradient matrices in back-propagation in training, but the functionalities of extracting knowledge from different components cannot be disparate for both fusions. Therefore, we design branches that produce different gradient flows from density maps of different scales and fuse them together to train a critical backbone module to instil density-awareness. Put figuratively. interconnections between branches and backbone, multisource gradients filtered by branches propagating backwards find their shortcuts to penetrate into the backbone network multilayeredly when supervision is applied. This is a process that enables the backbone to be trained to summarise useful information and gain more knowledge about the representation to improve itself.



350

351

352

353

354

355

356

357

358

359

360

361

362

363

364

365

366

367

368

384

387

388

389

390

391

Figure 3. Illustration of sum pooling operation for density map generation.

3.2. Network configuration

As shown in Figure 2, our proposed model consists of a straightforward down-sampling backbone and five branches interconnected to it. The backbone by itself has relatively low complexity. It functions as a deep CNN 371 regressor which takes the crowd image as input and predicts 372 the global count by regression. We design the network to 373 have input size of 384×512 to cater most aspect ratios in 374 practical uses, whereas arbitrary larger input image sizes 375 are tackled by division and combination. Correspondingly, 376 there are density maps of sizes $\{48 \times 64, 24 \times 32, 12 \times 377\}$ $16, 6 \times 8, 3 \times 4$ } produced.

Specifically, the backbone has a frontend which extracts 379 features from the input image. We transplant the first ten 380 convolution layers from VGG-16 as our frontend model for 381 faster training. The frontend produces feature maps of 8 times smaller spatial width and height relative to the input. 383 Following are some 3×3 convolution layers to further dwindle the size of feature maps until when its spatial dimension matches the input dimension of a 3×4 convolution layer entering to produce a 1×1024 vector. We use 3×3 convolution with strides of 2 to halve the spatial dimension of the feature maps in the backend. In addition, a standard 3×3 convolution layer is put between two downsampling layers to further deepen the network and to smooth the reduction of features.

As for branches, they work in an up-sampling manner. 392 Branches stemming from the last feature layer (1×1024) of 393 the backbone use 3×4 transposed convolution and then 4×4 394 transposed convolutions to up-sample the feature maps. To 395 the output of each transposed convolution layer, the deeper 396 feature maps from backbone with the same dimension are 397 appended. Together, they form the input to the next 398 transposed convolution layer. When this concatenation has 399 the spatial dimension that meets the target density map of the branch it is on, a 1×1 convolution comes in to

449

Module	Backbone	Branch 1	Branch 2	Branch 3	Branch 4	Branch 5
Input	Image 384×512×3	1×1024	1×1024	1×1024	1×1024	1×1024
1	VGG 16 Layers 1-10	Conv-tr-S1 3×4×1024×256	Conv-tr-S1 3×4×1024×256	Conv-tr-S1 3×4×1024×256	Conv-tr-S1 3×4×1024×256	Conv-tr-S1 3×4×1024×256
2	Conv-S1 3×3×512×256	Depth Concatenation	Depth Concatenation	Depth Concatenation	Depth Concatenation	Depth Concatenation
3	Conv-S2 3×3×256×512	Conv-tr-S2 4×4×512×256	Conv-tr-S2 4×4×512×256	Conv-tr-S2 4×4×512×256	Conv-tr-S2 4×4×512×256	Conv-S1 1×1×512×1
4	Conv-S1 3×3×512×256	Depth Concatenation	Depth Concatenation	Depth Concatenation	Depth Concatenation	
5	Conv-S2 3×3×256×512	Conv-tr-S2 4×4×512×256	Conv-tr-S2 4×4×512×256	Conv-tr-S2 4×4×512×256	Conv-S1 1×1×512×1	
6	Conv-S1 3×3×512×256	Depth Concatenation	Depth Concatenation	Depth Concatenation		
7	Conv-S2 3×3×256×512	Conv-tr-S2 4×4×512×256	Conv-tr-S2 4×4×512×256	Conv-S1 1×1×512×1		
8	Conv-S1 3×3×512×256	Depth Concatenation	Depth Concatenation			
9	Conv-S2 3×3×256×512	Conv-tr-S2 4×4×512×256	Conv-S1 1×1×512×1			
10	Conv-S1 3×3×512×256	Depth Concatenation				
11	Conv-S1 3×4×256×1024	Conv-S1 1×1×512×1				
12	Fc 1024×1					
Output	P. Count	P. Density Map 48×64	P. Density Map 24×32	P. Density Map 12×16	P. Density Map 6×8	P. Density Map 3×4

Table 1. Configuration of DeepCount network. In the table, Conv and Conv-tr mean convolution and transposed convolution respectively. The pattern $H \times W \times C \times C'$ represents the dimension of convolution kernel. S denotes strides.

reconstruct all channels to one to produce the density map prediction. At the end of the backbone, another 1×1 convolution (or fully connected layer) produces a scalar value, the global count prediction. We call our network DeepCount in short for deep CNN count regressor. Table 1 details the network configuration.

3.3. Generating ground truth density maps

To produce ground truth density maps for training, we first apply convolution by fixed Gaussian kernel with standard deviation $\sigma = 5$ (on the contrary of geometryadaptive kernel adopted in most works) to generate density map of the same resolution as the original image, before Sum Pooling is employed to produce different sizes of density maps. Sum pooling explicitly is summing all values inside a pooling window. Figure 3 illustrates this operation. As shown in Figure 3, five density maps are produced. Through sum pooling, element sum for all density maps created from one original density map stays unchanged; this sum is the ground truth count of the image.

3.4. Objective function

Labelling congested crowd data is indeed a painstaking task for human annotators, especially in some highly congested cases where the factual number of people is inevitably untraceable. This results in many annotations in congestions themselves being estimations, which means noise in the situation. Hence, L1-norm loss is adopted to enhance robustness against noise as well as to convey steady updates to the network. We first define our objective function as:

$$L(\Theta) = \frac{1}{2N} \sum_{n=1}^{N} \sum_{k=1}^{K} \sum_{i,j} |y'_{nk} - f(X_n, \Theta_k)|_{ij}$$
 (1)

474

475

476

478

479

480

481

482

483

488

489

491

492

493

494

where N is the size of the training batch, K ($K = 6 \& k \in$ {1,2,...,6}) enumerates outputs of all branches and the 484 global count regressor, y'_{nk} is the ground truth density map 485 (or the global count when k = 6), X_n is the input image and 486 Θ_k denotes all parameters in model f that contribute to 487 making the corresponding k_{th} prediction.

Given this objective function as basis, we add a multiplier β to accentuate the importance of the global count prediction on backbone (where k = 6). We notate it as a function of *k*:

$$B(k) = \begin{cases} \beta, & k = 6 \\ 1, & k \neq 6 \end{cases} \tag{2}$$

Moreover, we add another hyperparameter ω to 495 approximately adjust the loss to a reasonably small value 496 (<10). An L2 regularisation term is also added to the 497 function in an attempt to reduce overfitting. Hence, the 498 objective function finally becomes:

$$L(\boldsymbol{\theta}) = \left[\frac{1}{2N} \sum_{n=1}^{N} \sum_{k=1}^{K} \sum_{i,j} |y'_{nk} - f(X_n, \boldsymbol{\theta}_k)|_{ij} \cdot B(k)\right] \cdot \boldsymbol{\omega} + \frac{\lambda}{2} \|\boldsymbol{\theta}\|_2^2 \quad (3)$$

3.5. Implementation

VGG-16 model pretrained on ImageNet is used to initialise the frontend of the backbone. Therefore, input images are normalised in the same manner as how the VGG-16 model is trained. As for initialising the remaining part of the model, we use Xavier [33] initialisation for weights and a constant value 0 for biases. With the exception of the VGG-16 frontend where ReLU is the activation function, we set parametric ReLUs (leaky ReLU):

$$a(x) = \begin{cases} x, & x > 0 \\ \alpha x, & x \le 0 \end{cases} \tag{4}$$

following every convolution layer. We choose $\lambda = 1 \times$ 10^{-5} , $\omega = 1 \times 10^{-2}$ and $\beta = 16$ empirically for the loss function in equation (3), and $\alpha = 0.2$ for the activation parameter in equation (4) in light of experiments reported in [31]. We use Gradient Descent optimisation with momentum 0.9 and initial learning rate 1×10^{-4} to train our model, except for pretrained parameters in frontend where learning rate is divided by a factor of 2 to initially 5×10^{-5} . Batch size N is set to 32. A hundred epochs should be enough for training.

As alluded to above, to cope with images of varied sizes, we divide the original image to 384×512 crops to feed into our network. In inference, results from cropped images are to be merged to assemble the original ones again.

4. Evaluation

In this section, we report evaluation results yielded by our method introduced above. We evaluate our DeepCount network on four public datasets: Shanghai Tech Part A and Part B [4], UCF-QNRF [29] and Mall [13]. Training details for all datasets are the same as mentioned in implementation section (section 3.5). In order to make fair comparison with benchmark results, we do no more data augmentation than random cropping and mirroring during training.

4.1. Evaluation metrics

For evaluation, we compute mean-absolute error (MAE) and root-mean-squared error (RMSE):

$$MAE = \frac{1}{N} \sum_{i=1}^{N} |C_i - C_i^{GT}|$$
 (5)

$$MAE = \frac{1}{N} \sum_{i=1}^{N} |C_i - C_i^{GT}|$$

$$RMSE = \sqrt{\frac{1}{N} \sum_{i=1}^{N} ||C_i - C_i^{GT}||^2}$$
(6)

where N is the number of testing images, C_i and C_i^{GT} meaning predicted count and ground truth count respectively.

4.2. Shanghai Tech

Shanghai Tech [4] dataset includes Part A and Part B. Part A is the dataset for congested crowd counting. It has 241,677 annotations in 300 training images and 182 testing images with an average number 501. On the other hand, the relatively sparse Part B is separated into training set with 400 images and testing set with 316 images taken from streets in Shanghai. Our DeepCount model achieves stateof-the-art performance on both datasets. Test results are shown in Table 2.

550

551

552

553

554

555

556

557

558

559

560

561

562

563

564

565

566

567

568

569

570

571

572

573

580

581

582

583

584

585

586

587

588

589

590

591

592

593

	Part A		Part B	
Method	MAE	RMSE	MAE	RMSE
MCNN [4]	110.2	173.2	26.4	41.3
Switching CNN [5]	90.4	135.0	21.6	33.4
DecideNet [23]	-	-	20.75	29.42
CP-CNN [6]	73.6	106.4	20.1	30.1
ic-CNN [15]	68.5	116.2	10.7	16.0
CSRNet [16]	68.2	115.0	10.6	16.0
SANet [11]	67.0	104.5	8.4	13.6
DeepCount (ours)	65.2	112.5	7.2	11.3

Table 2. Test results on Shanghai Tech Part A and Part B

4.3. UCF-ONRF

The UCF-QNRF [29] dataset has a greater number of 574 annotations (1,251,642) in higher quality images of a wider 575 variety of scenes, including sparse and dense ones. There are extremely dense scenes in this dataset, so much so that a single image may have maximumly 12,865 of annotations 578 in UCF-QNRF. It is the most challenging one in terms of crowd density. Our method, to a great extent, outperforms current methods (see Table 3).

· ·	*	
Method	MAE	RMSE
Idrees et al. (2013) [3]	315	508
MCNN [4]	277	426
CMTL [24]	252	514
Switching CNN [5]	228	445
Resnet101[25]	190	277
Densenet201[26]	163	226
Idrees et al. (2018) [29]	132	191
DeepCount (ours)	95.7	167.1

Table 3. Test results on UCF-ONRF.

4.4. Mall

Unlike the three datasets aforementioned, images from Mall dataset [13] are surveillance video frames from a static 595 viewpoint at a same venue. There are 800 frames for 596 training and the other 1200 for testing. Since crowds in the 597 dataset are sparse, Mall is not as challenging as others. 598 Although previous methods have shown very promising 599 results on this dataset, we still evaluate our model on it to demonstrate its excellent performance on invariant scene and as well to make comparison with some detection-based

C	SRNet (backend)	•	De	DeepCount Branch 1			DeepCount (backend)		
Layer	Output	Million FLOPs	Layer	Output	Million FLOPs	Layer	Output	Million FLOPs	
Conv-s1 3×3×512×512	48×64×512	7248	Conv-tr-s1 3×4×1024×256	3×4×256	37	Conv-s1 3×3×512×256	48×64×256	3624	
Conv-s1 3×3×512×512	48×64×512	7248	Conv-tr-s2 4×4×512×256	6×8×256	101	Conv-s2 3×3×256×512	24×32×512	906	
Conv-s1 3×3×512×512	48×64×512	7248	Conv-tr-s2 4×4×512×256	12×16×256	403	Conv-s1 3×3×512×256	24×32×256	906	
Conv-s1 3×3×512×256	48×64×256	3624	Conv-tr-s2 4×4×512×256	24×32×256	1611	Conv-s2 3×3×256×512	12×16×512	226	
Conv-s1 3×3×256×128	48×64×128	906	Conv-tr-s2 4×4×512×256	48×64×256	6442	Conv-s1 3×3×512×256	12×16×256	226	
Conv-s1 3×3×128×64	48×64×64	226	Conv-s1-p0 1×1×512×1	48×64×1	2	Conv-s2 3×3×256×512	6×8×512	57	
Conv-s1 1×1×64×1	48×64×1	0.2				Conv-s1 3×3×512×256	6×8×256	57	
						Conv-s2 3×3×256×512	3×4×512	14	
						Conv-s1 3×3×512×256	3×4×256	14	
						Conv-s1-p0 3×4×256×1024	1×1×1024	3	
						Conv-s1-p0 (Fc) 1×1×1024×1	1	0.001	
Total		26500			8596			6034	

Table 5. Comparing between configurations and FLOPs of CSRNet and our DeepCount. Branch one (middle column) predicts the same size density maps as does CSRNet, while backbone predicts a global count without producing any density maps.

methods. (see Table 4).

Method	MAE	RMSE
R-FCN [27]	6.02	5.46
Faster R-CNN [28]	5.91	6.60
COUNT Forest [30]	4.40	2.40
Weighted VLAD [32]	2.41	9.12
DecideNet [23]	1.52	1.90
DeepCount (ours)	1.55	2.00

Table 4. Test results on Mall

5. Discussion

5.1. Capacity and velocity

Arguably, the more parameters a neural network has, the greater its potential is to have high capacity to model the underlying relationship of the random variables. Although many cases suggest otherwise, we do see the positive correlation between extra parameters and increments of performance [16, 19, 25, 38]. Be that as it may, we still tend to avoid expensive computation a larger network would bear in practice. Trading off between capacity and velocity has been a dilemma for long. Hereby, we explicate how the idea of our DeepCount network is able to pursue both capacity and velocity at the same time by comparing it with CSRNet [16] in whose paper Li et al. do persuasively argue about the effect of number of parameters and design efficiency.

CSRNet and our backbone network both have a straightforward design and use the same VGG-16 frontend, so the difference between the two lies in the backends, where CSRNet predicts the density map and our model predicts the global count. Assuming they receive the same 671 384×512×3 input (backends receive 48×64×channels 672 input), we detail their layer configuration with 673 corresponding output and computation cost of each layer in 674 Table 5. In addition, we add branch 1 which predicts the 675 density map as same as the one predicted by CSRNet to the 676 table. We compute computation cost in terms of number of floating-point operations (FLOPs) that happens throughout 678 a forward pass in the backend. Number of FLOPs of one 679 convolution layer is computed as:

$$FLOPs = H \cdot W \cdot C \cdot K_1 \cdot K_2 \cdot C' \tag{7}$$

where it depends multiplicatively upon output feature map size $H \times W$, convolution kernel size $K_1 \times K_2$, the number of output channels C, and the number of input channels C'. 684

We also measure number of parameters as well as frame- 685 per-second (FPS) for both networks (see Table 6). Run time 686 evaluation is performed on one NVIDIA Tesla P40 GPU. 687 As mentioned above, the backbone of our DeepCount 688 model can be a standalone network detached from the rest in inference, and thereby becomes a count regressor without computing the computationally expensive density maps, and noticeably, with overwhelming performance compared to other global count regression approaches.

Method	SHT Part B MAE	Million Parameters	FPS	Speedup
CSRNet	10.6	16.3	33	1×
DeepCount (ours)	7.2	21.4 (58.1 in total)	45	1.4×

Table 6. Comparing number of parameters and inference speed between CSRNet and the backbone of our DeepCount model.

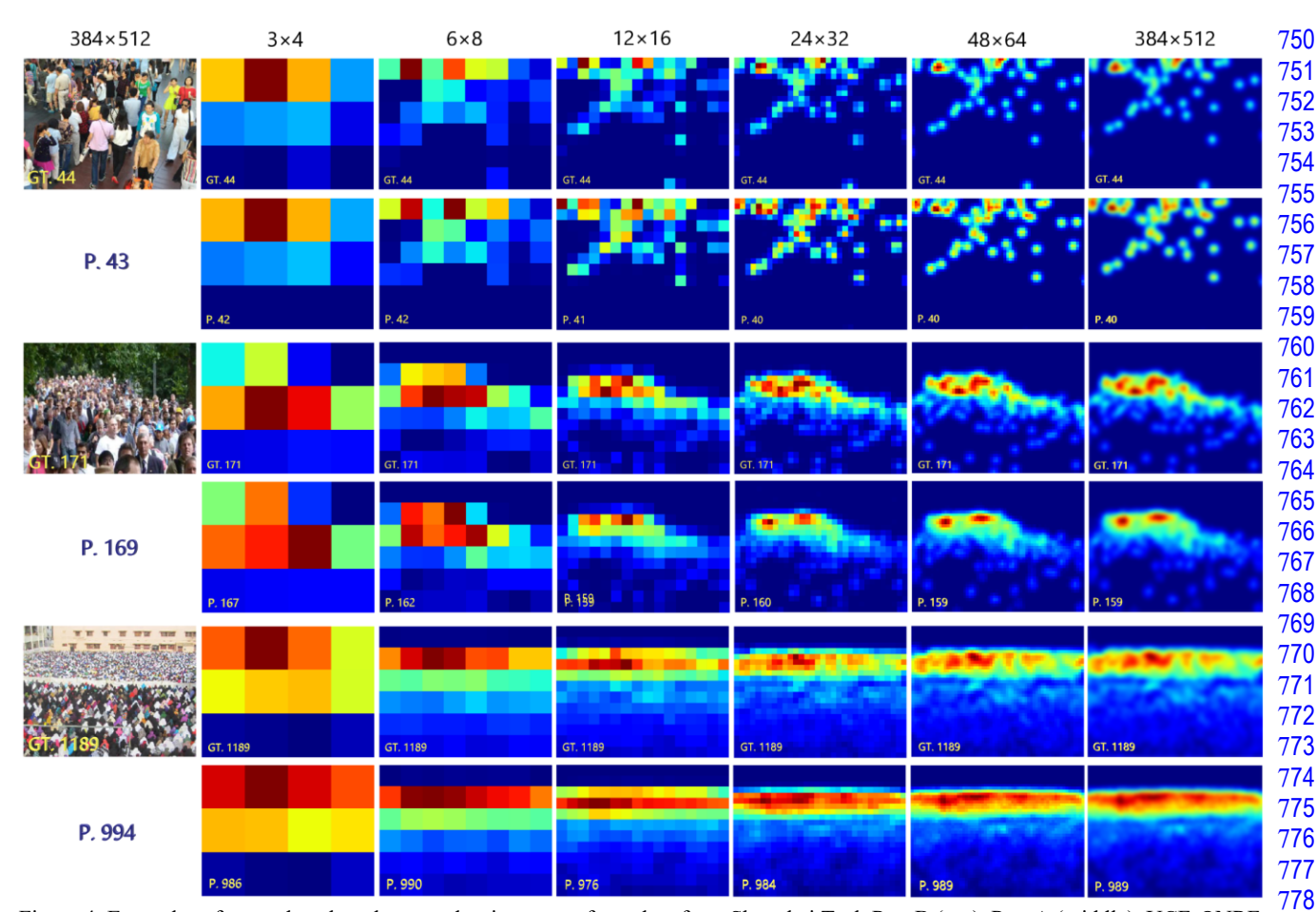


Figure 4. Examples of ground truth and output density maps of test data from Shanghai Tech Part B (top), Part A (middle), UCF-QNRF (bottom). Density maps in the row which starts with an image are the ground truths. The ones below are the predictions. The number in blue below the image is the predicted count by backbone alone. The last column shows original size ground truth density maps and predictions density maps up-sampled from outputs of branch one, up-sampling being done by bilinear interpolation and separable Gaussian filter.

As shown in Table 5 and Table 6, having a deeper and greater preponderance of parameters (58.1 million for training and 21.4 million for inference) though, our DeepCount backbone does count inferences with much less FLOPs and therefore in higher velocity, and perhaps more importantly, with higher accuracy. These quantitative results indicate our proposed DeepCount model has the ability of accommodating more variations while making faster and better prediction. This implies its nature of outstanding capacity and efficiency.

5.2. Comparison on branches

Each branch produces a density map of a particular resolution at its end. As we have obtained the global count regressed by backbone, we can as well integrate the output density map to make count prediction like common density map-based methods. In the following, we compare predictions made in terms of MAE between branches. Besides, we compute FLOPs for each branch to analyse

their computational cost. Results are shown in Table 7.

779

780

781

782

783

794

796

797

As shown, the fact that branches that are able to produce 784 larger density maps give inferior predictions on the count 785 compared to those producing smaller ones suggests that the 786 higher the resolution of density map, the harder it is to be 787 optimised. Immediate reasons for this may be that larger 788 density maps are sparser and usually awash with noise 789 caused mostly by annotations of large-scale heads. Our 790 method avoids predicting the count relying merely on 791 density maps, but exploits useful information from them to 792 rather train the global count regressor. This allows more 793 accurate predictions to be achieved.

In spite of extra computation, there are situations in 795 which density maps, which give information about the distribution, become a requirement. Our DeepCount model can make direct count inference with backbone in its full speed while optionally producing density maps of multiple resolutions. User can choose smaller density maps to reduce computational expensiveness or larger ones to give more

	Branch 1	Branch 2	Branch 3	Branch 4	Branch 5	Backbone
Output Size	48×64	24×32	12×16	6×8	3×4	1×1
Shanghai Tech Part A	79.2	73.4	69.7	66.7	65.8	65.2
Shanghai Tech Part B	9.7	8.9	8.0	7.4	7.2	7.2
UCF-QNRF	193.3	185.0	155.3	112.3	96.9	95.7
Mall	4.74	2.89	2.46	1.77	1.56	1.55
Million FLOPs	6034	2152	541	138	38	-

Table 7. Comparing between outputs on different branches.

illuminating impression about the crowd distribution. Using bilinear interpolation and separable Gaussian filter, the largest density map can be efficiently up-sampled to original resolution for high-definition display. Figure 4 shows our predicted density maps compared to their ground truths.

5.3. Significance of gradients

Gradients are considered crucial to the achievement of our model. Hence, we detail more experiments to further cast light on the importance of them. Since ReLU has derivatives:

$$a(x)'_{ReLU} = \begin{cases} 1, & x > 0 \\ 0, & x < 0 \end{cases}$$
 (8)

, where gradients in half of its activation space are set to zero, the resulting sparse gradient matrices would hinder propagation of gradient flow and counterproductively cause a large part of the network underused. Instead, Parametric ReLU has derivatives:

$$a(x)'_{PReLU} = \begin{cases} 1, & x > 0 \\ \alpha, & x < 0 \end{cases}$$
 (9)

with non-zero gradients in all quadrants which allow the network to fully learn. Table 8 shows results of training a network with all ReLU activations in comparison with our baseline network. As shown in Table 8, when gradients are sparse, the capability of the network drops.

Activation	SHT Part B MAE
ReLU	8.8
PReLU	7.2

Table 8. Comparing results between using ReLU (sparse gradients) and PReLU (full gradients).

Also, the idea of being density-aware by gradient fusion is to leverage gradients sourced from supervision of multiscale density maps. In ablation experiments (see Table 9 for the results), as we detach branches one by one from the

Ablation	SHT Part B MAE
No ablation	7.2
Branch 1 ablated	7.4
Branches 1-2 ablated	7.7
Branches 1-3 ablated	8.2
Branches 1-4 ablated	8.3
Branches 1-5 ablated	9.1

Table 9. Ablation on branches.

largest to the smallest in training, the backbone receives less gradients in each case, and then the trend of performance degradation becomes more and more apparent.

850

851

853

854

855

856

857

859

860

861

862

863

864

869

870

883

884

885

886

887

889

891

892

893

895

897

898

By means of this, we are now safer to conclude that the abundance of gradients has advantageous influence on our network and parameters in branches are indeed instrumental in the training of backbone. Giant as it may be, the network of branches is not a concern in deployment for inferences. Unless training efficiency is also in a serious consideration, having a rationally greater number of parameters in this auxiliary module should be deemed 867 innocuous as long as performance does not remain stagnant. 868

6. Conclusion

In this paper, we have discussed advantages and limitations of current crowd counting methods, in light of which we propose a novel DeepCount network to be both fast and precise on count prediction and flexible on density map generation. State-of-the-art performance on public datasets evidence the effectiveness of our method. We reckon it is also worth mentioning that our method 877 prevailed to a great extend over current state-of-the-arts on 878 a much larger and more practical dataset with 14k images 879 from BaiduStar2018 [39] competition of crowd counting 880 which could be a more convincing evidence of its 881 accomplishments. Our code and models will be publicly 882 available at https://github.com/[anonymised].

References

- W. Ge and R. T. Collins, "Marked point processes for crowd counting," 2009 IEEE Conference on Computer Vision and 888 Pattern Recognition, Miami, FL, 2009, pp. 2913-2920.
- H. Idrees, K. Soomro and M. Shah, "Detecting Humans in 890 Dense Crowds Using Locally-Consistent Scale Prior and Global Occlusion Reasoning," in IEEE Transactions on Pattern Analysis and Machine Intelligence, vol. 37, no. 10, pp. 1986-1998, 1 Oct. 2015.
- H. Idrees, I. Saleemi, C. Seibert and M. Shah, "Multi-source 894 [3] Multi-scale Counting in Extremely Dense Crowd Images," 2013 IEEE Conference on Computer Vision and Pattern 896 Recognition, Portland, OR, 2013, pp. 2547-2554.
- Y. Zhang, D. Zhou, S. Chen, S. Gao and Y. Ma, "Single-Image Crowd Counting via Multi-Column Convolutional Neural Network," 2016 IEEE Conference on Computer 899 Vision and Pattern Recognition (CVPR), Las Vegas, NV, 2016, pp. 589-597.

- [5] D. B. Sam, S. Surya and R. V. Babu, "Switching Convolutional Neural Network for Crowd Counting," 2017 IEEE Conference on Computer Vision and Pattern Recognition (CVPR), Honolulu, HI, 2017, pp. 4031-4039.
- [6] V. A. Sindagi and V. M. Patel, "Generating High-Quality Crowd Density Maps Using Contextual Pyramid CNNs," 2017 IEEE International Conference on Computer Vision (ICCV), Venice, 2017, pp. 1879-1888.
- [7] C. Zhang, H. Li, X. Wang and Xiaokang Yang, "Cross-scene crowd counting via deep convolutional neural networks," 2015 IEEE Conference on Computer Vision and Pattern Recognition (CVPR), Boston, MA, 2015, pp. 833-841.
- [8] V. A. Sindagi and V. M. Patel, "A survey of recent advances in cnn-based single image crowd counting and density estimation," Pattern Recognition Letters, no. 107, pp. 3-16, 2018.
- [9] M. S. Zitouni, H. Bhaskar, J. Dias, and M. E. Al-Mualla, "Advances and trends in visual crowd analysis: A systematic survey and evaluation of crowd modelling techniques," Neurocomputing, no. 186, pp. 139-159, 2016.
- [10] Viola, Jones and Snow, "Detecting pedestrians using patterns of motion and appearance," Proceedings Ninth IEEE International Conference on Computer Vision, Nice, France, 2003, pp. 734-741 vol.2.
- [11] X. Cao, Z. Wang, Y. Zhao, and F. Su, "Scale aggregation network for accurate and efficient crowd counting," in Proceedings of the European Conference on Computer Vision (ECCV), pp. 734-750, 2018.
- [12] J. Gall, A. Yao, N. Razavi, L. Van Gool and V. Lempitsky, "Hough Forests for Object Detection, Tracking, and Action Recognition," in IEEE Transactions on Pattern Analysis and Machine Intelligence, vol. 33, no. 11, pp. 2188-2202, Nov. 2011.
- [13] K. Chen, C. C. Loy, S. Gong, and T. Xiang, "Feature mining for localised crowd counting," in British Machine Vision Conference (BMVC), vol. 1, no. 2, pp. 3, 2012.
- [14] A. B. Chan, Zhang-Sheng John Liang and N. Vasconcelos, "Privacy preserving crowd monitoring: Counting people without people models or tracking," 2008 IEEE Conference on Computer Vision and Pattern Recognition, Anchorage, AK, 2008, pp. 1-7.
- [15] V. Ranjan, H. Le, M. Hoai, "Iterative crowd counting," in Proceedings of the European Conference on Computer Vision (ECCV), pp. 270-285, 2018.
- [16] Y. Li, X. Zhang and D. Chen, "CSRNet: Dilated Convolutional Neural Networks for Understanding the Highly Congested Scenes," 2018 IEEE/CVF Conference on Computer Vision and Pattern Recognition, Salt Lake City, UT, 2018, pp. 1091-1100.
- [17] Z. Ma and A. B. Chan, "Crossing the Line: Crowd Counting by Integer Programming with Local Features," 2013 IEEE Conference on Computer Vision and Pattern Recognition, Portland, OR, 2013, pp. 2539-2546.
- [18] C. Wang, H. Zhang, L. Yang, L. Si, and X. Cao, "Deep people counting in extremely dense crowds." in Proceedings of the 23rd ACM international conference on Multimedia, 2015, pp. 1299-1302.
- [19] K. Simonyan and A. Zisserman, "Very deep convolutional networks for large-scale image recognition," arXiv:1409.1556 [cs.CV], Sep. 2014.

- [20] D. Kong, D. Gray and Hai Tao, "A Viewpoint Invariant 950 Approach for Crowd Counting," 18th International 951 Conference on Pattern Recognition (ICPR'06), Hong Kong, 952 2006, pp. 1187-1190. 953
- [21] M. Rodriguez, I. Laptev, J. Sivic and J. Audibert, "Densityaware person detection and tracking in crowds," 2011 955 International Conference on Computer Vision, Barcelona, 2011, pp. 2423-2430.

956

960

965

969

983

987

989

990

991

993

994

995

998

- [22] M. Li, Z. Zhang, K. Huang and T. Tan, "Estimating the 957 number of people in crowded scenes by MID based 958 foreground segmentation and head-shoulder detection," 2008 19th International Conference on Pattern Recognition, Tampa, FL, 2008, pp. 1-4.
- [23] J. Liu, C. Gao, D. Meng and A. G. Hauptmann, "DecideNet: 961 Counting Varying Density Crowds Through Attention 962 Guided Detection and Density Estimation," 2018 IEEE/CVF 963 Conference on Computer Vision and Pattern Recognition, 964 Salt Lake City, UT, 2018, pp. 5197-5206.
- [24] V. A. Sindagi and V. M. Patel, "CNN-Based cascaded multitask learning of high-level prior and density estimation for crowd counting," 2017 14th IEEE International Conference 967 on Advanced Video and Signal Based Surveillance (AVSS), 968 Lecce, 2017, pp. 1-6.
- [25] K. He, X. Zhang, S. Ren and J. Sun, "Deep Residual Learning 970 for Image Recognition," 2016 IEEE Conference on Computer Vision and Pattern Recognition (CVPR), Las Vegas, NV, 2016, pp. 770-778.
- [26] G. Huang, Z. Liu, L. v. d. Maaten and K. Q. Weinberger, 973 "Densely Connected Convolutional Networks," 2017 IEEE 974 Conference on Computer Vision and Pattern Recognition 975 (CVPR), Honolulu, HI, 2017, pp. 2261-2269.
- [27] J. Dai, Y. Li, K. He, and J. Sun. "R-fcn: Object detection via region-based fully convolutional networks," in Advances in neural information processing systems, 2016, pp. 379-387.
- [28] S. Ren, K. He, R. Girshick and J. Sun, "Faster R-CNN: 979 Towards Real-Time Object Detection with Region Proposal 980 Networks," in IEEE Transactions on Pattern Analysis and 981 Machine Intelligence, vol. 39, no. 6, pp. 1137-1149, 1 June 982 2017.
- [29] H. Idrees, M. Tayyab, K. Athrey, D. Zhang, S. Al-Maadeed, N. Rajpoot and M. Shah, "Composition loss for counting, density map estimation and localization in dense crowds," in 985 Proceedings of the European Conference on Computer 986 Vision (ECCV), pp. 532-546, 2018.
- [30] V. Pham, T. Kozakaya, O. Yamaguchi and R. Okada, 988 "COUNT Forest: CO-Voting Uncertain Number of Targets Using Random Forest for Crowd Density Estimation," 2015 IEEE International Conference on Computer Vision (ICCV), Santiago, 2015, pp. 3253-3261.
- [31] B. Xu, N. Wang, T. Chen, and M. Li, "Empirical evaluation 992 of rectified activations in convolutional network," arXiv:1505.00853 [cs.LG], 2015.
- [32] B. Sheng, C. Shen, G. Lin, J. Li, W. Yang and C. Sun, "Crowd Counting via Weighted VLAD on a Dense Attribute Feature Map," in IEEE Transactions on Circuits and Systems 996 for Video Technology, vol. 28, no. 8, pp. 1788-1797, Aug. 997
- [33] X. Glorot, and Y. Bengio, "Understanding the difficulty of 999 training deep feedforward neural networks," in Proceedings of the thirteenth international conference on artificial intelligence and statistics, pp. 249-256, 2010.

1000	[24] T. 71 D. N	1050
1000	[34] T. Zhao, R. Nevatia and B. Wu, "Segmentation and Tracking of Multiple Humans in Crowded Environments," in IEEE	1050
1001	Transactions on Pattern Analysis and Machine Intelligence,	1051
1002	vol. 30, no. 7, pp. 1198-1211, July 2008.	1052
1003	[35] L. Liu, H. Wang., G. Li, W. Ouyang, and L. Lin, "Crowd	1054
1004	counting using deep recurrent spatial-aware network,"	1055
1005	arXiv:1807.00601 [cs.CV], 2018. [36] D. B. Sam and R. V. Babu, "Top-down feedback for crowd	1056
1007	counting convolutional neural network," in Thirty-Second	1057
1007	AAAI Conference on Artificial Intelligence, 2018.	1057
1000	[37] Z. Shi et al., "Crowd Counting with Deep Negative	1059
1010	Correlation Learning," 2018 IEEE/CVF Conference on	1060
1011	Computer Vision and Pattern Recognition, Salt Lake City,	1061
1012	UT, 2018, pp. 5382-5390. [38] A. G. Howard, M. Zhu, B. Chen, D. Kalenichenko, W. Wang,	1062
1013	T. Weyand, M. Andreetto, and H. Adam, "Mobilenets:	1063
1014	Efficient convolutional neural networks for mobile vision	1064
1015	applications," arXiv:1704.04861 [cs.CV], 2017.	1065
1016	[39] "Developer Competition 2018," Star.baidu.com, 2018.	1066
1017	[Online]. Available: http://star.baidu.com/developer.html. [Accessed: 21- Mar- 2019]	1067
1018	[Accessed, 21- Mai- 2017]	1068
1019		1069
1020		1070
1021		1071
1022		1072
1023		1073
1024		1074
1025		1075
1026		1076
1027		1077
1028		1078
1029		1079
1030		1080
1031		1081
1032		1082
1033		1083
1034		1084
1035		1085
1036		1086
1037		1087
1038		1088
1039		1089
1040		1090
1041		1091
1042 1043		1092 1093
1043		1093
1044		1094
1045		1095
1040		1096
1047		1097
1049		1099
		1000